# Supplementary Information

## Local differences in neuronal activation level decorrelate spatially coherent fluctuations in gamma rhythms

Kaushik J. Lakshminarasimhan, Nikos K. Logothetis, Georgios A. Keliris

**Contents**

## Supplementary Figures

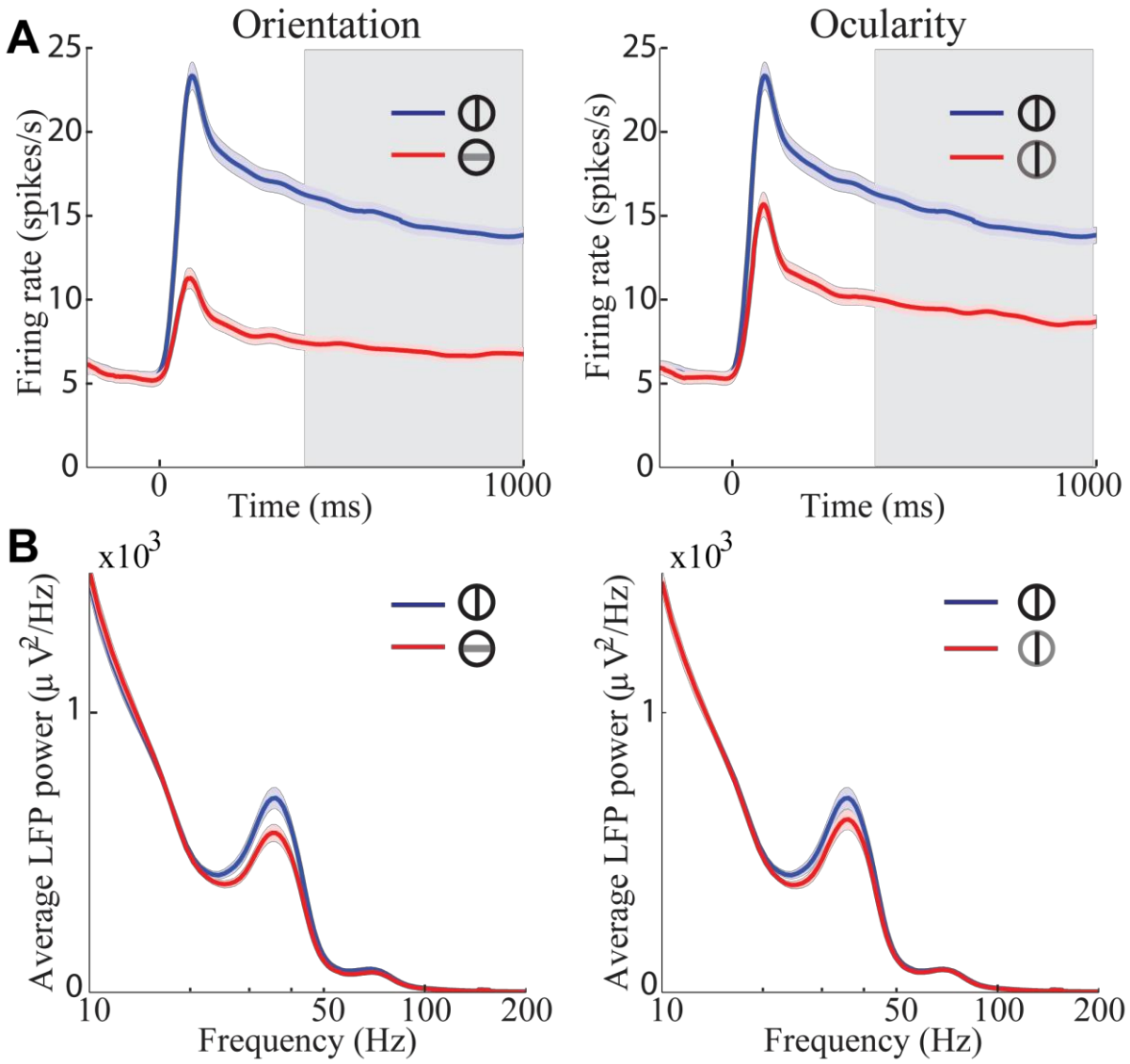


**Figure S1. Changes in firing rates and LFP spectra across the population of singleunits/LFPs that exhibited significant gamma-band SFC. (A)** Time-course of firing rate averaged across 166 singleunits corresponding to all 400 spike-LFP pairs (see main text). **(B)** LFP power spectral density (PSD) averaged across LFPs recorded from 184 sites corresponding to the 400 spike-LFP pairs (For clarity, only frequencies above 10 Hz are shown). Blue and red traces denote responses to preferred and non-preferred orientations of the singleunits respectively. Shaded regions denote ±1 standard error in mean (SEM).

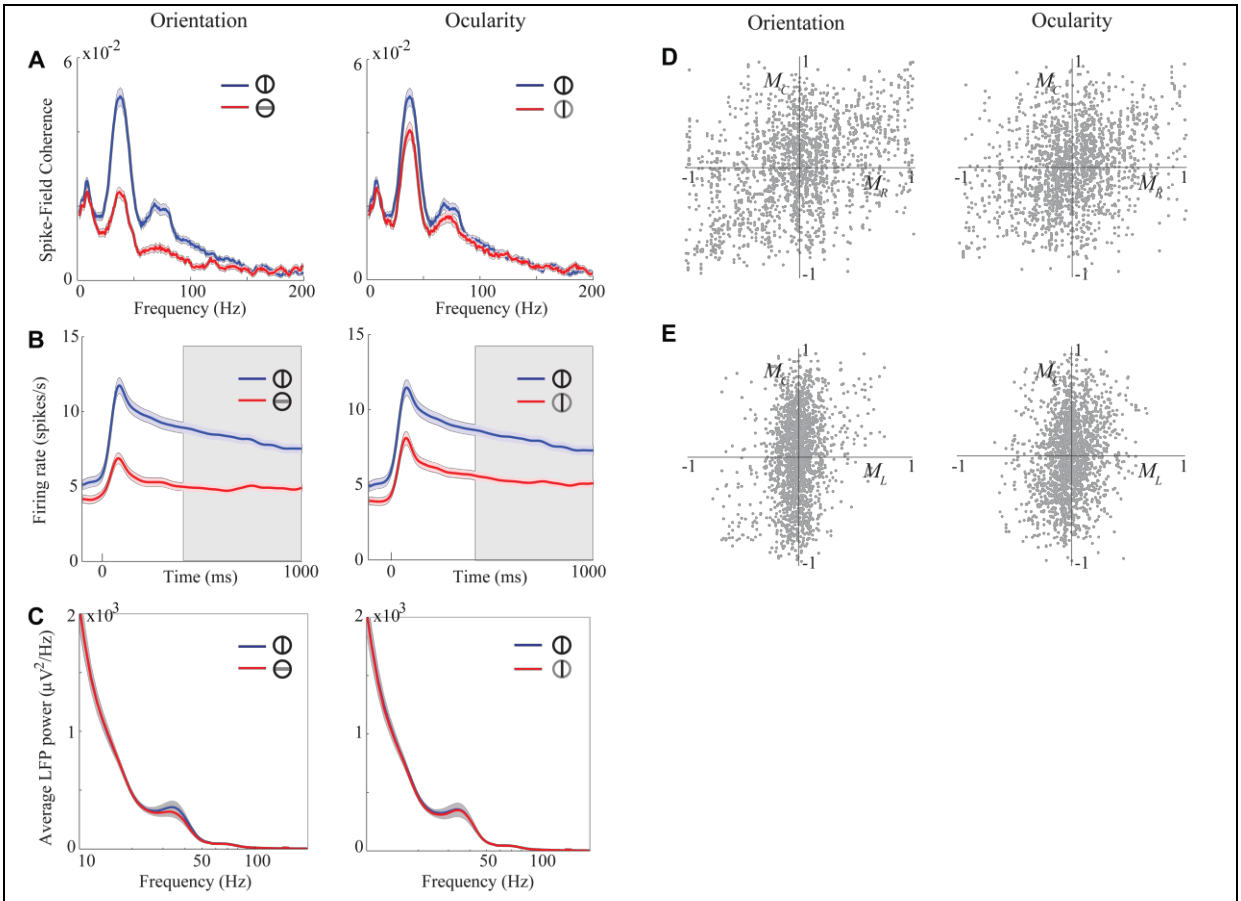


**Figure S2. Changes in Firing rates, LFP spectra, and SFC across the full dataset. (A)** SFC averaged across all spike-LFP pairs in the complete dataset (*n*=1927), regardless of whether the gamma-band coherence was significant. Blue and red traces denote responses to preferred and non-preferred orientations/eye of the singleunits respectively. Shaded regions denote ±1 standard error in mean (SEM). **(B)** Time-course of firing rate averaged across all visually responsive singleunits (*n*=610). **(C)** LFP power spectral density (PSD) averaged across LFPs from the corresponding electrodes (*n*=332). **(D)** Rate modulation indices ($M_R$) of orientation selectivity of the single-units from each spike-LFP pair (gray dot) plotted against the corresponding coherence modulation indices ($M_C$). **(E)** Similar to (D), but showing modulations in gamma-band SFC ($M_C$) and gamma-band LFP power ($M_L$).

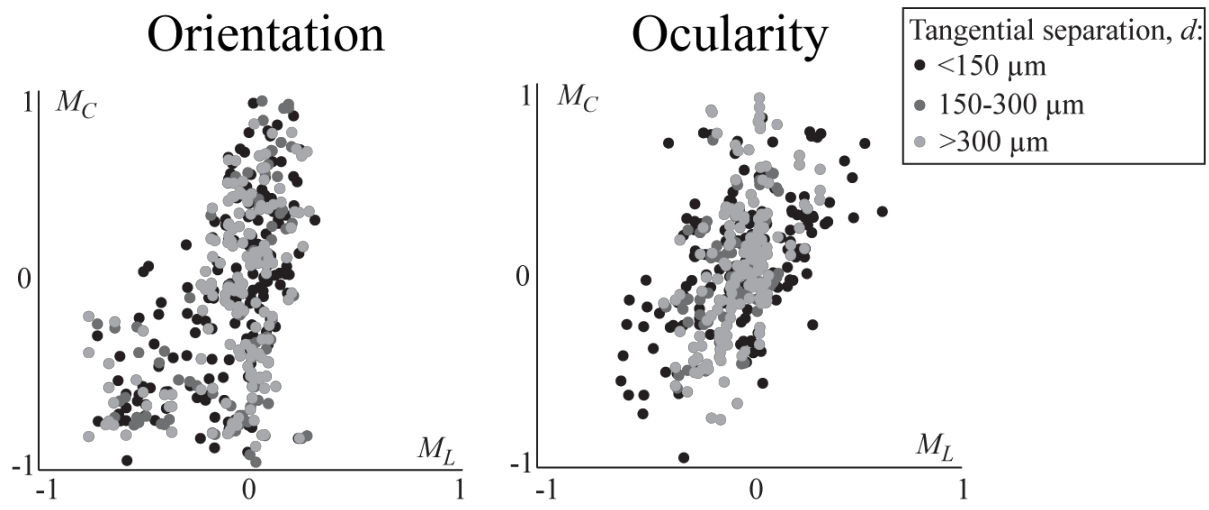


**Figure S3. Correlation between neuronal synchrony and LFP does not depend on distance.** Spike-LFP pairs were categorised into three groups based on the distance between the electrode site from which spikes were isolated and the site of the LFP recording. Stimulus-related modulations in gamma-band LFP, $M_L$, and modulations in neuronal synchrony, $M_C$ are shown for changes in both orientation (left) and ocularity (right). Neither the correlation coefficient nor slope of linear regression differed systematically between the three groups under both pairs of stimulus conditions. Orientation: 95% confidence intervals (CI) for Correlation coefficients: $r_{d1} = [0.45\ 0.66]$, $r_{d2} = [0.26\ 0.61]$, $r_{d3} = [0.29\ 0.54]$. 95% CI for Regression slopes: $\beta_{d1} = [2.3\ 3.8]$, $\beta_{d2} = [3.0\ 6.4]$, $\beta_{d3} = [2.7\ 6.0]$. Ocularity: Correlation coefficients: $r_{d1} = [0.39\ 0.62]$, $r_{d2} = [0.21\ 0.58]$, $r_{d3} = [0.35\ 0.59]$. Regression slopes: $\beta_{d1} = [1.4\ 2.5]$, $\beta_{d2} = [2.7\ 8.5]$, $\beta_{d3} = [3.5\ 6.7]$. Tangential separation between electrode sites from which spikes and LFP were recorded (in $\mu m$): $d1 < 150$, $150 < d2 < 300$, $d3 > 300$.

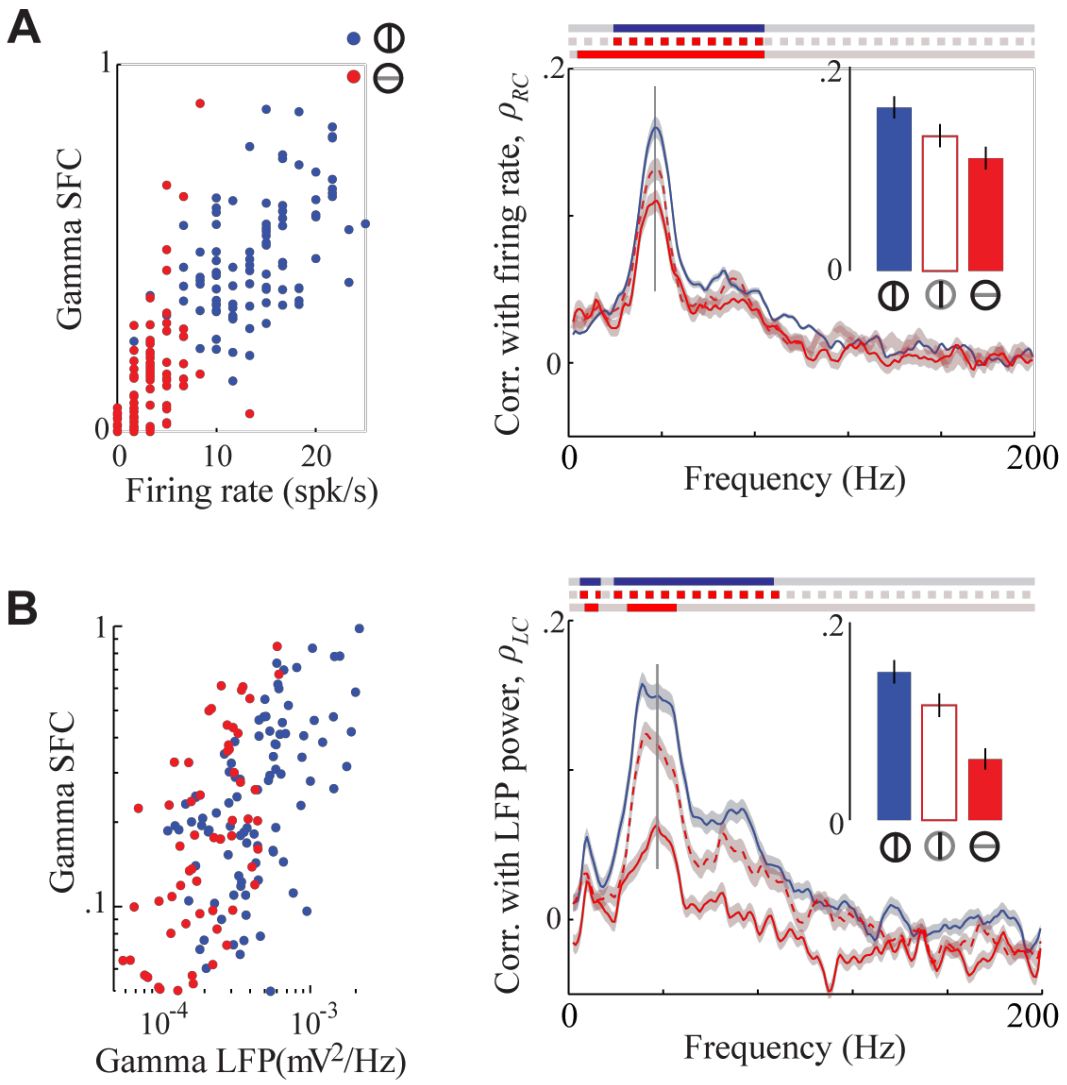


**Figure S4. Correlated variability of neuronal synchrony with firing rate and LFP persists in the absence of stimulus change.** Single-trial pseudo spike-field coherences (pSFC) were estimated using the procedure outlined in Methods. **(A)** Left: Gamma-band pSFC of an example singleunit plotted against its firing rate for each individual trial for a pair of stimulus conditions. Right: Spearman's correlation coefficient between pSFC and firing rates ($\rho_{RC}$) across trials corresponding to three stimulus conditions, averaged across all spike-LFP pairs. Shaded regions correspond to ±1 SEM. *p*-values of correlation coefficients of individual spike-LFP pairs were combined using Fisher's method to obtain a chi-squared ($\chi^2$) statistic at each frequency. Line segments on top have been darkened to indicate the range of frequencies for which $\chi^2$ exceeded a certain threshold (corresponding to $p<10^{-3}$). These segments included the gamma frequency in each stimulus condition. Inset: Correlation coefficients at the peak gamma frequency (vertical line in main figure) were significantly different between stimulus conditions (see text). **(B)** Left: Gamma-band pSFC of an example singleunit plotted against gamma-band LFP power at a neighboring site for individual trials for a pair of stimulus conditions. Right: Population averages of trial-by-trial correlations between pSFC and LFP power ($\rho_{LC}$).

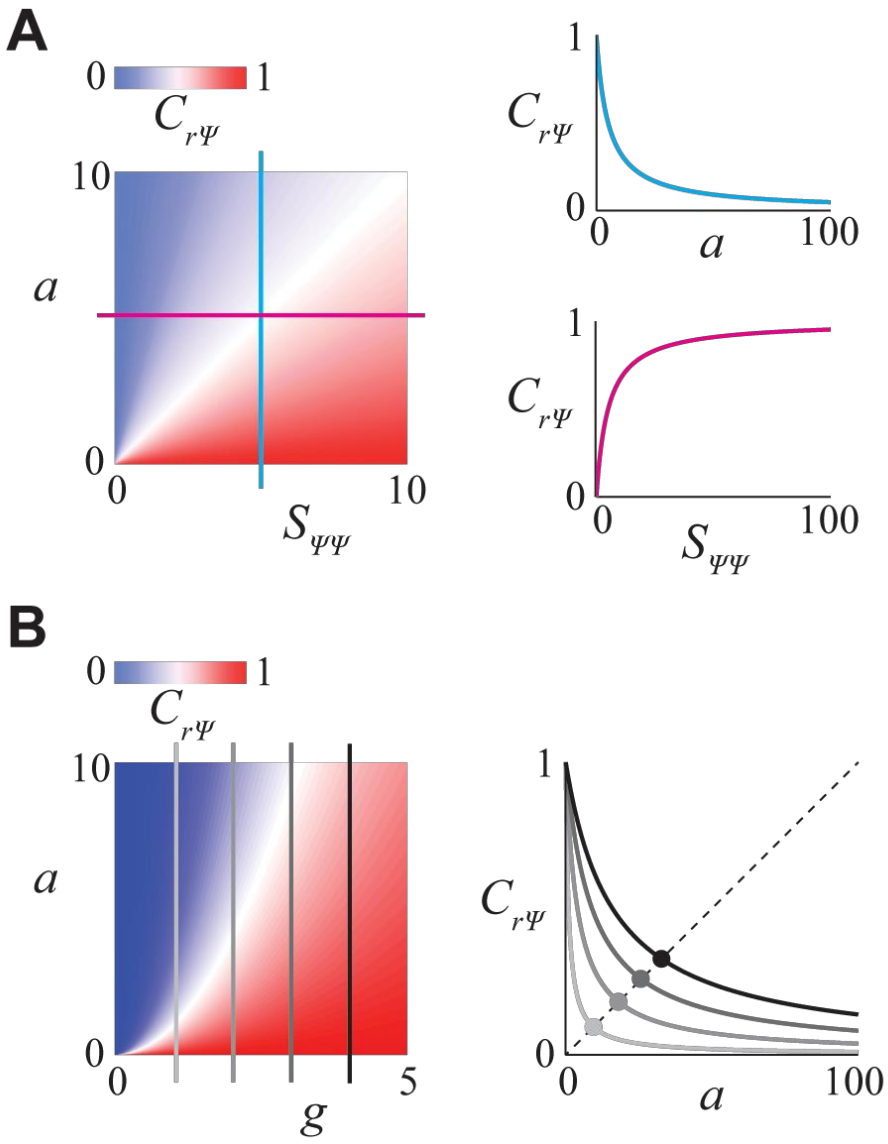


**Figure S5. Dependence of neuronal synchrony on synchronous input, activation level, and sensitivity. (A) Left:** Synchrony of a model neuron described in Equation (1) was quantified using spike-field coherence $\mathbf{C_{r\psi}}$ and plotted for various combinations of activation level $a$ and the strength of synchronous input $\mathbf{S_{\psi\psi}}$. **Right:** Neuronal synchrony decreases with activation level (cyan, shown here for $\mathbf{S_{\psi\psi}} = 5$), and increases with strength of the synchronous input (purple, shown here for $a = 5$). **(B) Left:** Synchrony of the same neuron plotted for various combinations of activation level $a$ and sensitivity $g$. **Right:** Synchrony as a function of activation level for four different values of sensitivity ($g$=1,2,3,4 indicated by vertical lines on the left panel). Activation-dependent increase in sensitivity can result in positive correlations between synchrony and activation level (dashed line).

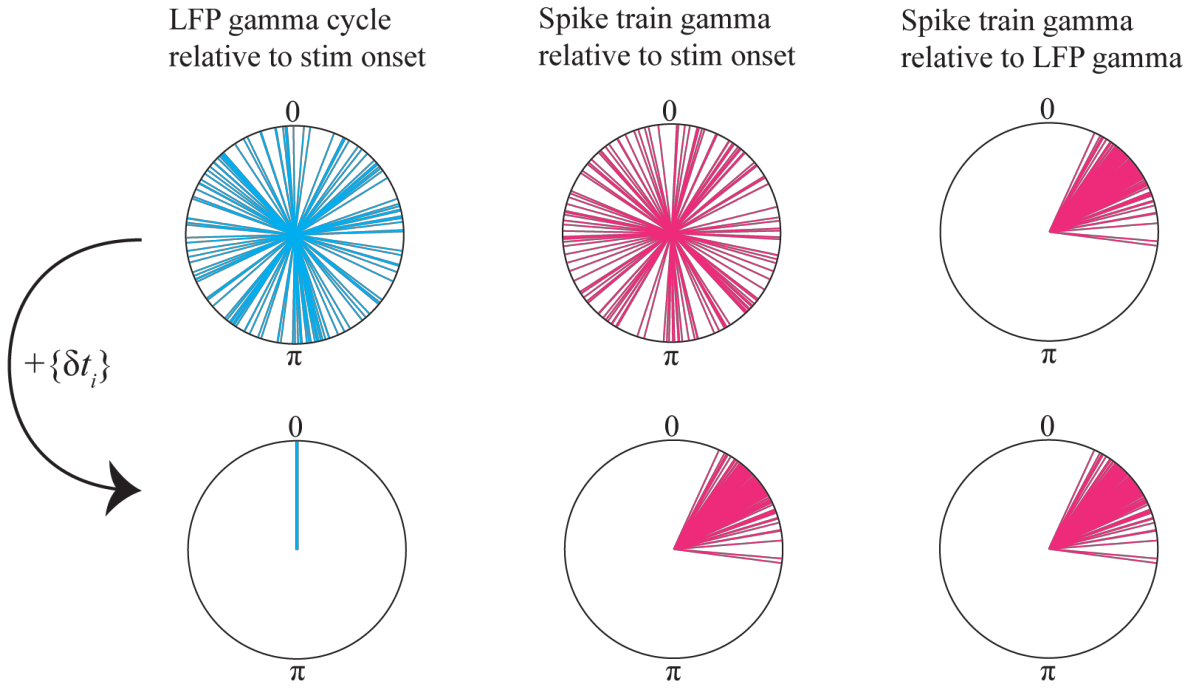


**Figure S6. Shifting spike trains and LFP did not affect phase-relationship between them. Top panels:** Phase relationships prior to the shifting procedure. Left: Gamma cycle of the LFP (shown here for a representative site) has no consistent phase relationship with stimulus onset. Middle: Gamma cycle of the spike trains were also not phase-locked to stimulus onset. Consequently, averaging across trials w.r.t stimulus onset would typically destroy oscillatory activities in the LFP and spike trains. Right: Spike-trains exhibited significant phase-locking with gamma rhythms of the LFP from the corresponding trials indicating strong spike-field coherence (SFC). **Bottom panels:** Phase relationships following the shifting procedure. $\delta t_i$ denotes the amount which the $i^{th}$ trial was shifted by. Left: LFP traces from all trials were shifted so as to align the phase of their gamma cycles. Consequently for the resulting traces, gamma phase measured w.r.t stimulus onset was identical across trials. Middle: Spike train from each trial was shifted by the same amount as the LFP trace. Since spikes were tightly phase-locked to the LFP rhythms, they now also exhibit significant phase-locking w.r.t stimulus onset. Right: The above procedure preserved the phase-relationship between spike trains and LFP (and thus also the SFC) because they were both shifted by the same amount.

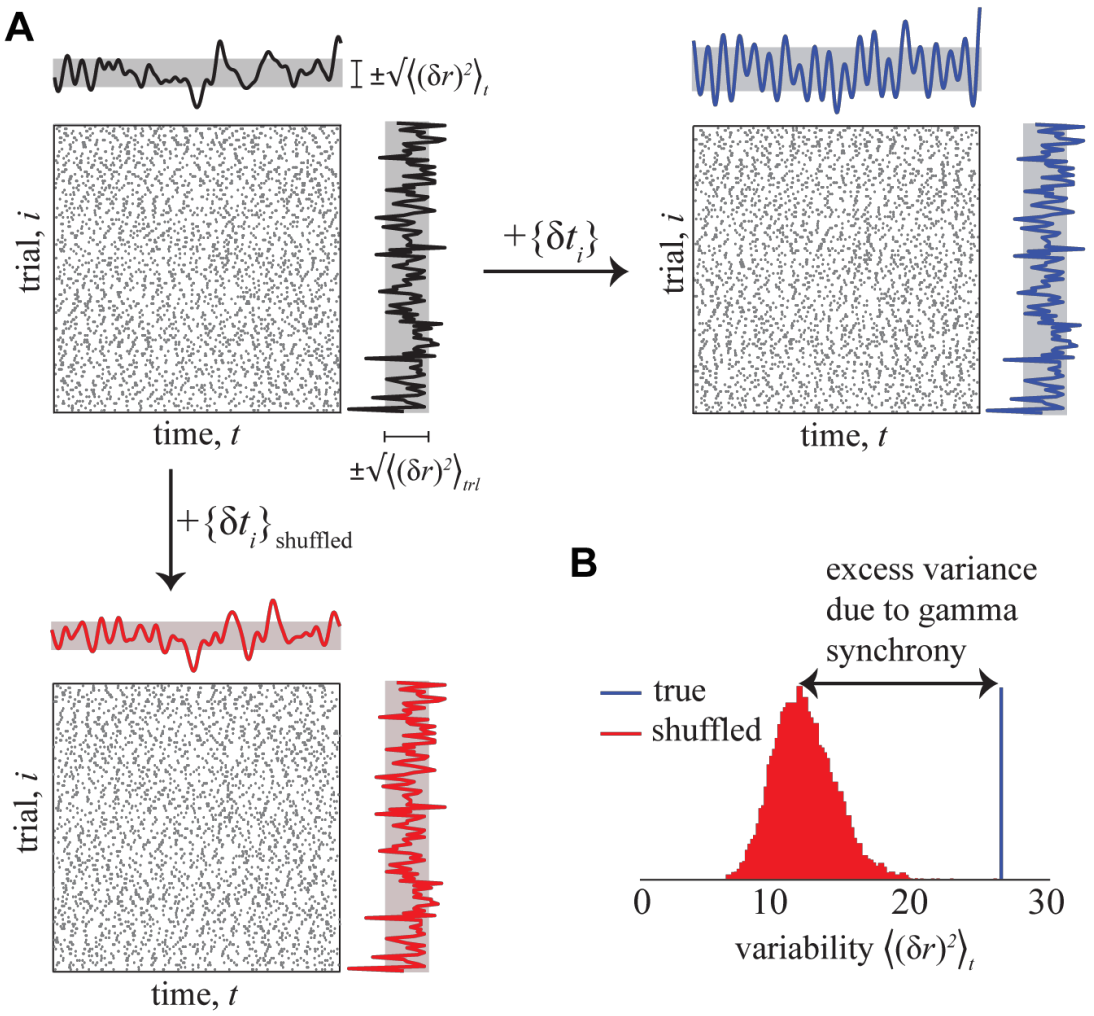


**Figure S7. Partitioning temporal variability of spiking process. (A)** Raster plots showing spike times of a representative neuron across trials prior to the shifting procedure (top left panel), following the shifting procedure (see Figure S4) in which the $i^{th}$ trial was shifted by $\delta t_i$ (top right panel), and following a surrogate procedure in which the elements of $\{\delta t_i\}$ were shuffled before shifting (bottom left panel). Only activities between 400 and 1000ms after the onset of stimulus are shown. In all cases, the marginals on top represent the timecourse of trial-averaged firing rates while those to the right represent firing rate on each trial averaged across time. Shaded regions denote ±1 standard deviation of these marginal traces. Since the shifting procedure does not affect spike counts, the right marginals are identical in all cases. On the other hand, this procedure affects the temporal relationship between trials thereby changing the timecourse of trial-averaged firing rates as seen from the differences in marginals on top. **(B)** The distribution of temporal variability of 10,000 surrogates obtained by the shuffling procedure (red) had a mean that was significantly less than the temporal variability estimated by the shifting procedure (blue). This difference corresponds to the excess variability due to synchronous gamma-rhythmic input, which was divided by the strength of synchronous input to estimate neuronal sensitivity to synchrony according to equation (7).

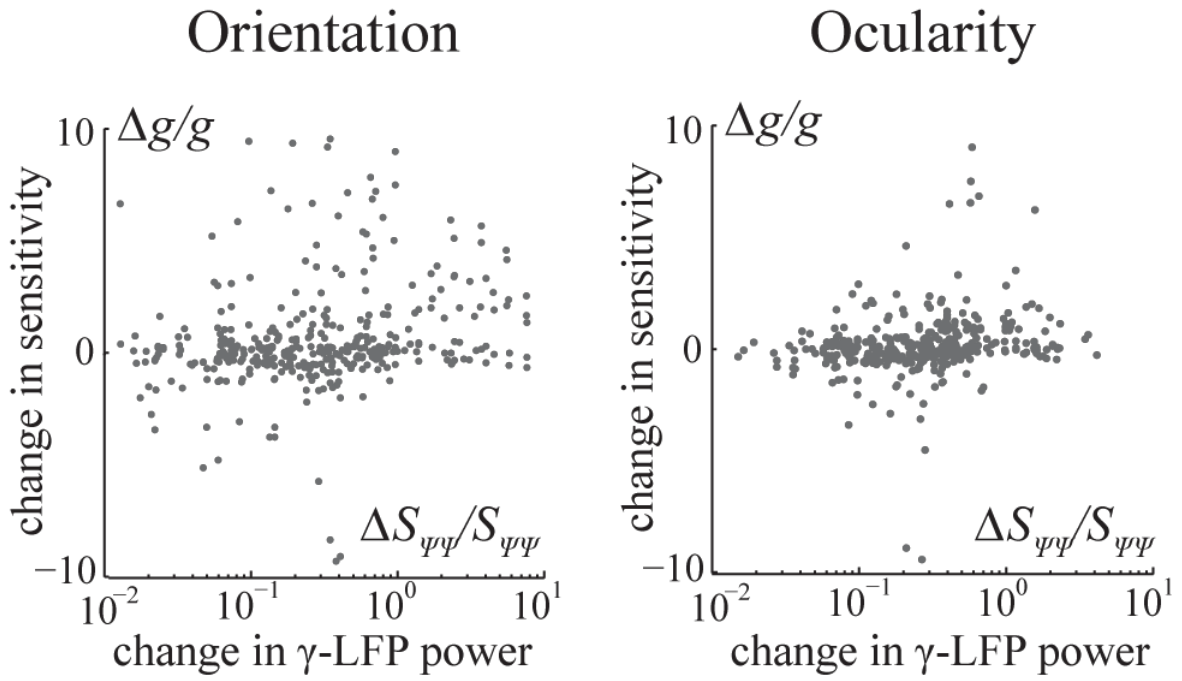


**Figure S8. Sensitivity was not correlated with the strength of synchronous input.** Left: Fractional change in sensitivity $\Delta g/g$ induced by change in stimulus orientation was not correlated with fractional change in strength of synchronous input $\Delta S_{\psi\psi}/S_{\psi\psi}$ (determined by changes in gamma-band power of the LFP). Each circle corresponds to one spike-LFP pair. Right: Changes in sensitivity and gamma-band LFP were also uncorrelated for the pair of ocularity conditions.

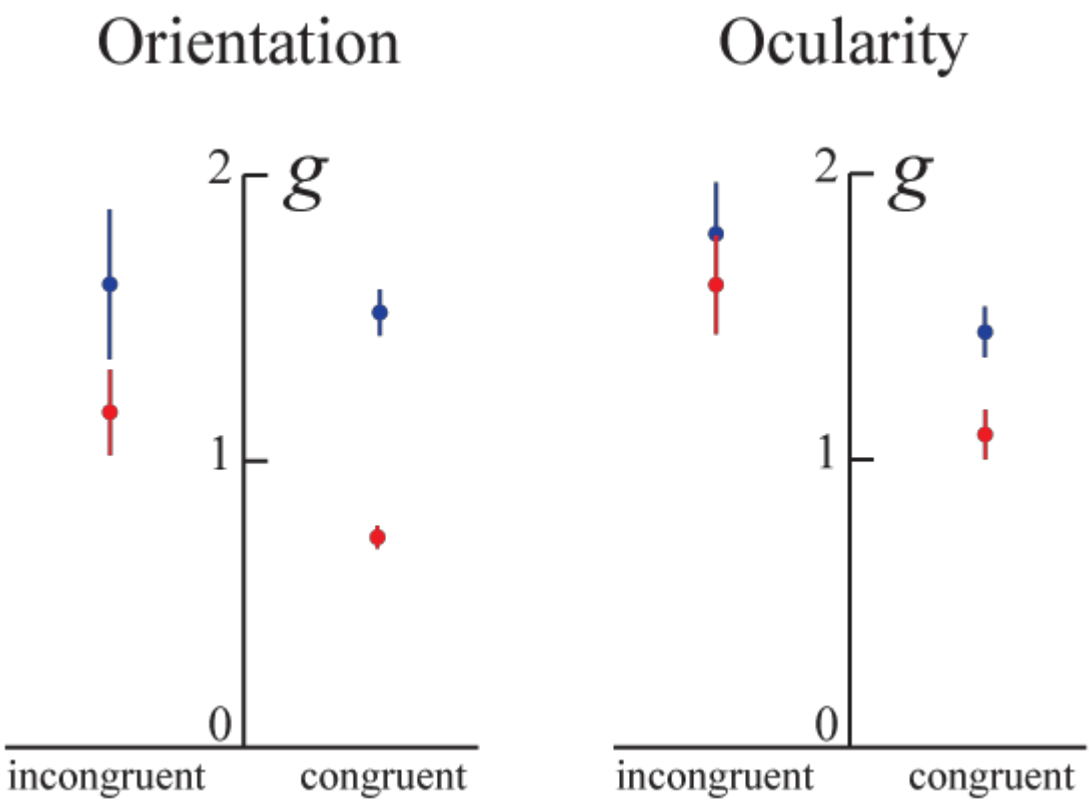


**Figure S9. Changes in sensitivity in congruent and incongruent neuronal populations.** Neurons were categorised based on whether stimulus-induced changes in neuronal synchrony were congruent or incongruent with changes in mean firing rate. For both orientation (left panel) as well as ocularity (right panel) conditions, changes in sensitivity were found to be significant for the population of congruent, but not incongruent neurons. Error bars denote ±1 SEM.

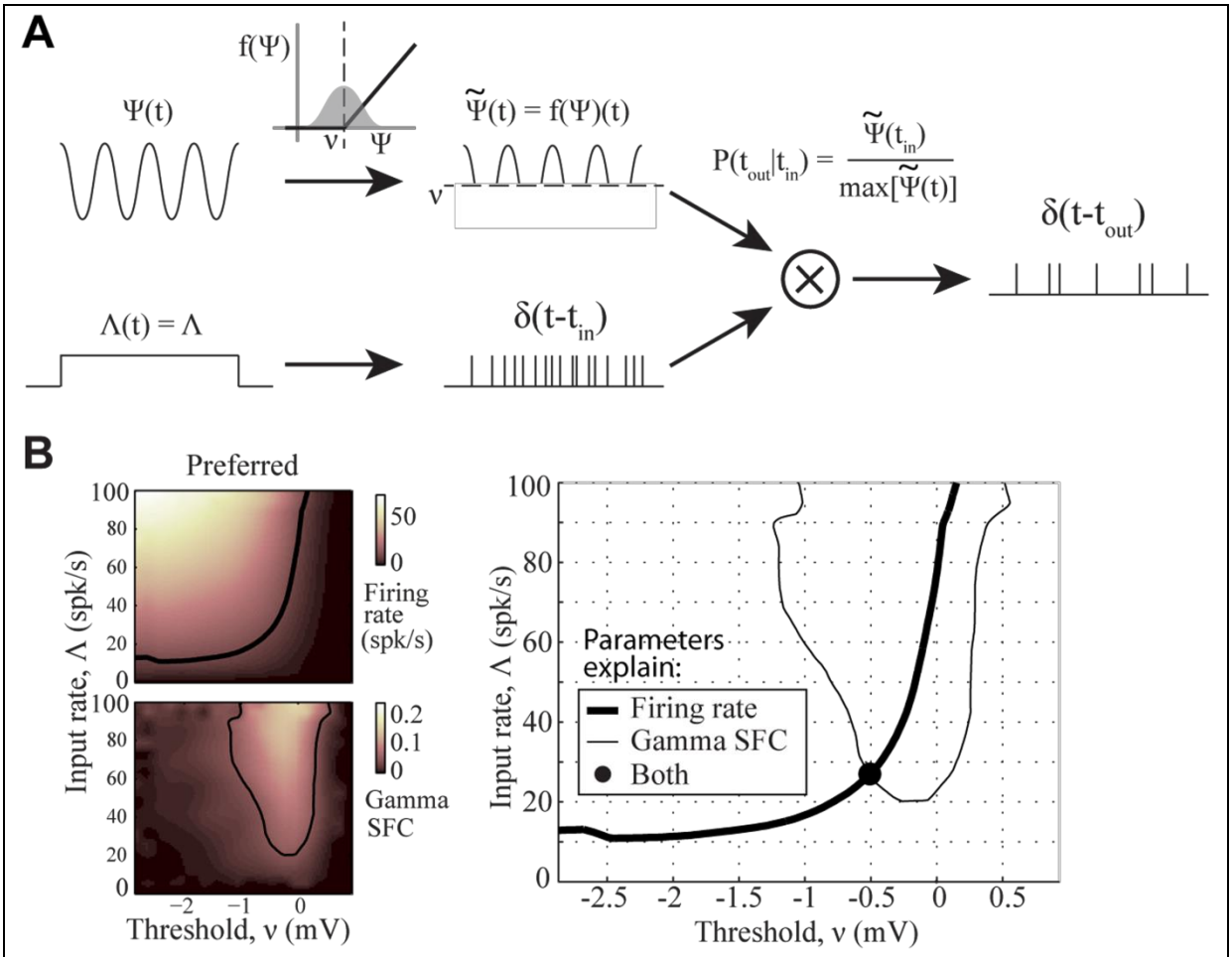


**Figure S10. Threshold linear model. (A) Model schematic.** Input spike train $\delta(t - t_{in})$ generated from a homogeneous Poisson process with mean Λ spikes $s^{-1}$, is modulated by an inhomogeneous Poisson process Ψ′(t) constructed from the LFP signal Ψ(t) following a threshold-linear transformation f, to produce output spike train $\delta(t-t_{out})$. $P(t_{out}|t_{in})$ corresponds to the probability of an input spike being transmitted to the output. **(B) Model fitting:** *Left*: LFPs Ψ recorded during the presentation of the stimulus, was transformed using a threshold-linear operation with threshold ν and then used to modulate the input spike trains to a representative singleunit. Both Λ and ν were varied across a range of values, and the resulting output spike trains were used to generate predictions for firing rates (top panel) and gamma-band SFCs (bottom panel) across the Λ-ν parameter space. The overlaying contours correspond to the set of parameters that yielded experimentally observed values. *Right*: The model parameter for the spike-LFP pair was inferred from the point of intersection (solid circles) of the contour lines corresponding to the neuronal firing rate and gamma-band SFC observed experimentally for that spike-LFP pair.

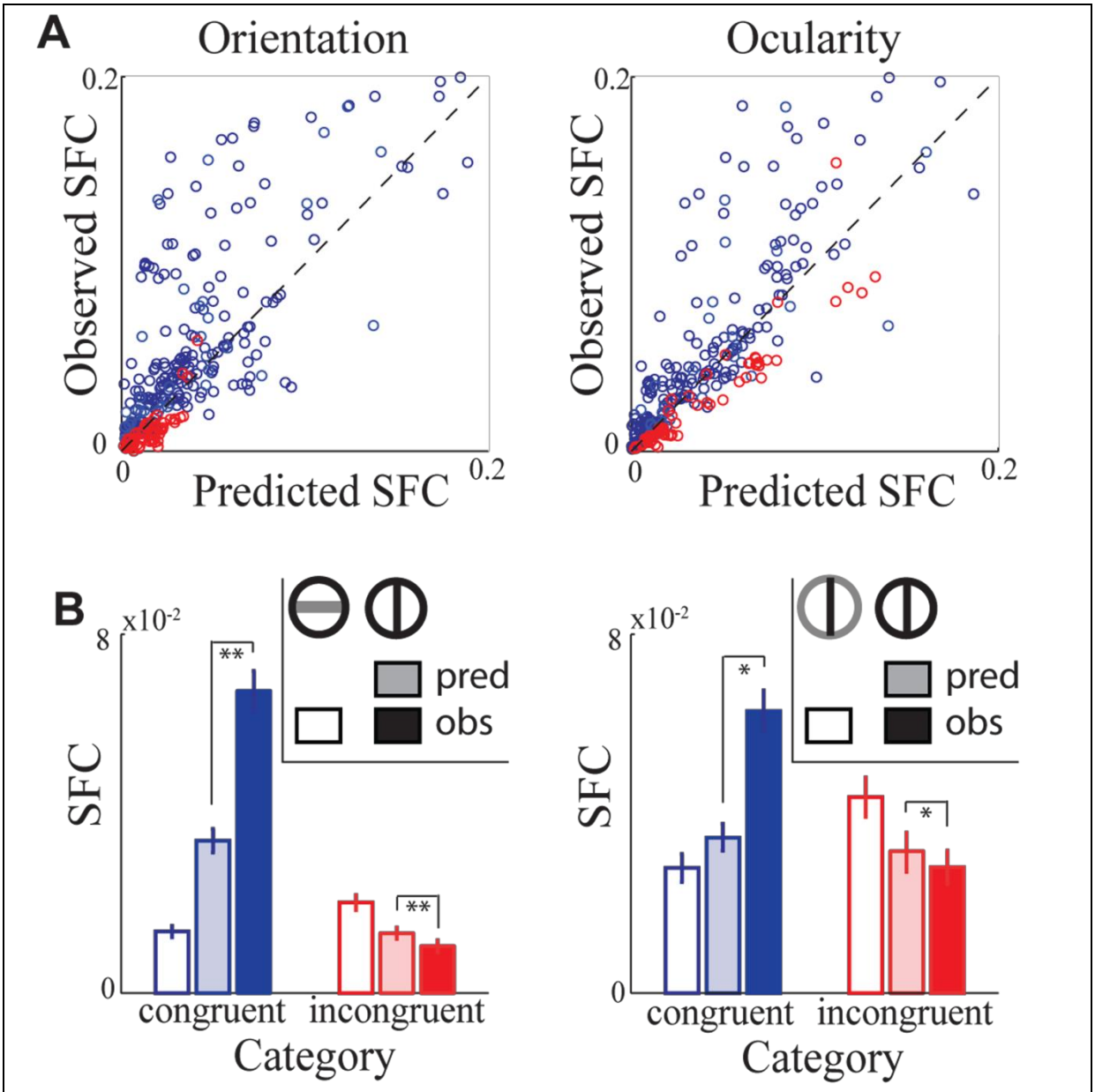


**Figure S11. Static threshold model fails to predict increase in SFC.** We divided the spike-LFP pairs in our dataset into two groups: congruent (blue) and incongruent (red) depending on whether their spike-field coherence (SFC) increased or decreased with firing rate. **(A)** For each spike-LFP pair, gamma-band SFC for the preferred orientation was predicted by fixing the threshold at values inferred from fitting the data for the corresponding nonpreferred orientations. These predictions are plotted against experimentally observed SFC. **(B)** Similar to (A), but for the pair of ocularity conditions. **(C)** Mean values of the predicted and true coherences in response to preferred orientation for congruent (blue) and incongruent (red) neurons. Coherence of congruent and incongruent neurons are significantly underestimated and overestimated, respectively. **(D)** Similar to (C), but for the pair of ocularity conditions. (*p<0.05, **p<0.005).

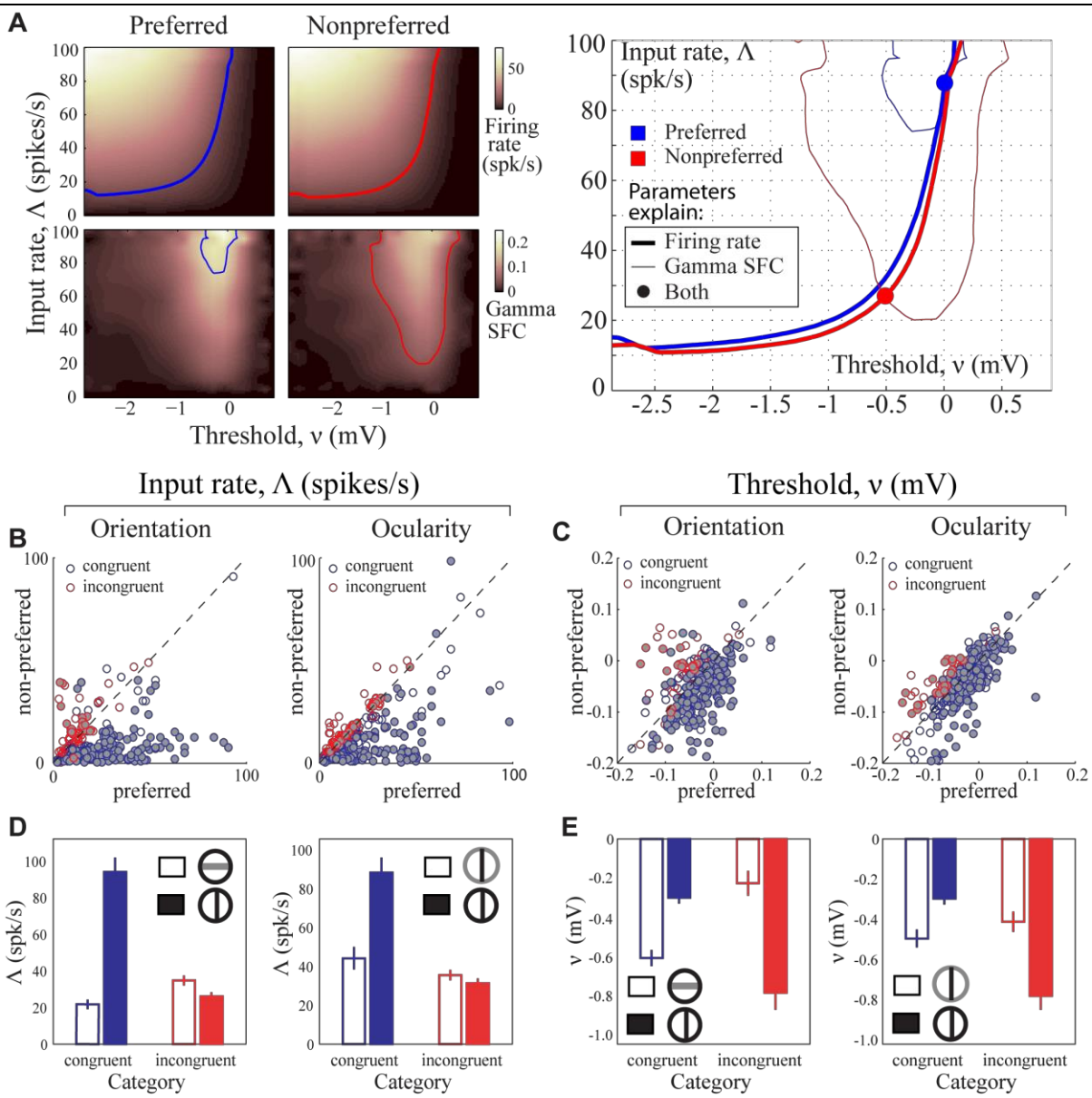


**Figure S12. Effect of stimulus on model parameters. (A)** The input rate Λ and threshold ν were fit to data from the preferred and non-preferred stimulus conditions separately (*left*), yielding model parameters for each stimulus condition. **(B)** For each spike-LFP pair, input intensity (Λ) inferred for the grating of preferred orientation (pEpO) is plotted against those inferred for the nonpreferred orientation (pEnpO). Pairs for which SFC increased with firing rate ('congruent') are shown in blue while those for which SFC decreased with firing rate ('incongruent') are shown in red. Filled circles are the ones for which change in SFC with stimulus was significant (permutation test $p<0.01$). **(B,D)** *Left:* Average input intensities in response to nonpreferred (red) and preferred (blue) orientations for both categories of spike-LFP pairs. Error bars denote 1 SEM. *Right:* Similar plots for the pair ocularity conditions. **(C,E)** Same as (B), but for the threshold parameter (ν).

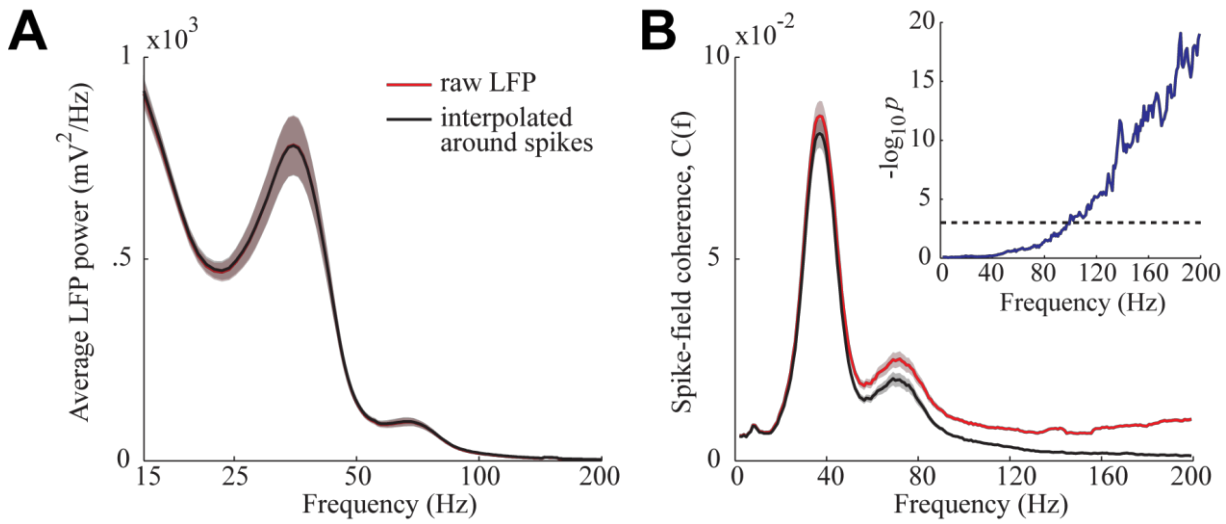


**Figure S13. LFP processing did not contaminate gamma-band SFC estimates.** For every spike-LFP pair in which spikes and LFPs were obtained from the same site, 4ms LFP segments were removed around the time of each spike and filled with cubic spline interpolation in order to avoid spurious coherences. **(A)** LFP power spectral density before (red) and after the interpolation procedure (black), averaged across all spike-LFP pairs in which spikes and LFPs were recorded from the same electrode. This procedure did not affect the power spectral density of LFP (for clarity, only frequencies above 15 Hz are shown). **(B)** Average SFCs estimated using raw (red) and interpolated (black) LFPs. Inset shows that the interpolation procedure resulted in a significant reduction of SFC estimates as compared to those derived from using raw LFPs (dashed line: $p$=0.001; Wilcoxon rank-sum test) only at frequencies above 100 Hz suggesting that – (*i*) Artifactual coherences are present, but only at frequencies above 100 Hz, and (*ii*) Our results would be valid even without the correction procedure, since SFCs around 40 Hz were not affected. Shaded regions represent ±1 SEM.

## Supplementary notes

We considered a linear model in which neuronal response $\mathbf{r}$ was related to asynchronous activation $\mathbf{A}$ with mean $a$, and rhythmic input $\boldsymbol{\psi}$ according to:

$$\mathbf{r} = \mathbf{A} + g\boldsymbol{\psi}$$

where $g$ denotes the sensitivity to rhythmic input such that greater sensitivities would lead to more efficient transfer of coherence by the neuron. We used rhythms in the local field potential recordings as a proxy for $\boldsymbol{\psi}$. Therefore the spike-field coherence (SFC) of this model neuron is essentially the coherence between the spiking process $\mathbf{r}$ and input $\boldsymbol{\psi}$. In the following, we show that, when sensitivity $g$ is fixed, SFC increases with the strength of $\boldsymbol{\psi}$ but decreases with mean firing rate $\langle\mathbf{r}\rangle$. We then derive constraints on sensitivity that allow for positive correlations between SFC and firing rates in our linear model.

Let $\tilde{\mathbf{r}}$, $\widetilde{\mathbf{A}}$, and $\widetilde{\boldsymbol{\psi}}$ denote the Fourier transformations of $\mathbf{r}$, $\mathbf{A}$, and $\boldsymbol{\psi}$ respectively, and $\tilde{\mathbf{r}}^*$, $\widetilde{\mathbf{A}}^*$, and $\widetilde{\boldsymbol{\psi}}^*$ their complex conjugates. We then have:

$$\tilde{\mathbf{r}} = \widetilde{\mathbf{A}} + g\widetilde{\boldsymbol{\psi}}$$

$$\Leftrightarrow \quad \langle\tilde{\mathbf{r}}\widetilde{\boldsymbol{\psi}}^*\rangle = \langle\widetilde{\mathbf{A}}\widetilde{\boldsymbol{\psi}}^*\rangle + g\langle\widetilde{\boldsymbol{\psi}}\widetilde{\boldsymbol{\psi}}^*\rangle$$

$$= g\langle\widetilde{\boldsymbol{\psi}}\widetilde{\boldsymbol{\psi}}^*\rangle$$

since $\mathbf{A}$ and $\boldsymbol{\psi}$ are uncorrelated processes. Coherence spectrum $\mathbf{C_{r\psi}}$ between $\mathbf{r}$ and $\boldsymbol{\psi}$ is then given by (Jarvis and Mitra, 2000):

$$\frac{\langle\tilde{\mathbf{r}}\widetilde{\boldsymbol{\psi}}^*\rangle^2}{\langle\tilde{\mathbf{r}}\tilde{\mathbf{r}}^*\rangle\langle\widetilde{\boldsymbol{\psi}}\widetilde{\boldsymbol{\psi}}^*\rangle} = \frac{g^2\langle\widetilde{\boldsymbol{\psi}}\widetilde{\boldsymbol{\psi}}^*\rangle^2}{\langle\tilde{\mathbf{r}}\tilde{\mathbf{r}}^*\rangle\langle\widetilde{\boldsymbol{\psi}}\widetilde{\boldsymbol{\psi}}^*\rangle} = \frac{g^2\mathbf{S_{\psi\psi}}}{\mathbf{S_{AA}} + g^2\mathbf{S_{\psi\psi}}}$$

where $\mathbf{S_{\psi\psi}}$ and $\mathbf{S_{AA}}$ denote the power spectral densities of $\boldsymbol{\psi}$ and $\mathbf{A}$ respectively. If $\mathbf{A}$ is a Poisson process with mean $a$, then $\mathbf{S_{AA}}(f) = a \;\forall\; f$ (Gerstner and Kistler, 2002) so that:

$$\mathbf{C_{r\psi}} = \frac{g^2\mathbf{S_{\psi\psi}}}{a + g^2\mathbf{S_{\psi\psi}}} \tag{S1}$$

It follows that $\frac{\partial \mathbf{C_{r\psi}}}{\partial \mathbf{S_{\psi\psi}}} = ag^2\left(a + g^2\mathbf{S_{\psi\psi}}\right)^{-2} > 0$, and $\frac{\partial \mathbf{C_{r\psi}}}{\partial \langle \mathbf{r} \rangle} = \frac{\partial \mathbf{C_{r\psi}}}{\partial a} = -g^2\mathbf{S_{\psi\psi}}\left(a + g^2\mathbf{S_{\psi\psi}}\right)^{-2} < 0$ for all $g \neq 0$. Thus, for fixed values of sensitivity $g$, SFC of the model neuron is expected to increase with gamma-band power of the LFP ($\mathbf{S_{\psi\psi}}$), and decrease with mean firing rate ($\langle \mathbf{r} \rangle$) (**Figure S5A**). Nevertheless, since $\frac{\partial \mathbf{C_{r\psi}}}{\partial g} = 2ag\mathbf{S_{\psi\psi}}\left(a + g^2\mathbf{S_{\psi\psi}}\right)^{-2}$, SFC is an increasing function of $|g|$. Thus an activation-dependent increase in the magnitude of sensitivity can potentially cause SFC to strictly increase with firing rate (**Figure S5B**). In particular, it can be shown that this is guaranteed under the condition that:

$$\left|\frac{\partial g}{\partial a}\right| > \left|\frac{g}{2a}\right| \tag{S2}$$

If sensitivity is an increasing function of $a$ such that $g \propto a^p$ for some scalar $p$, then equation (S2) is satisfied for all $p > 1/2$.

# Supplementary references


Jarvis MR, Mitra PP (2000) Sampling properties of the spectrum and coherency of sequences of action potentials. Neural Computation 13:717–749.

Gerstner W, Kistler WM (2002) Spiking Neuron Models (Maass W, C B, eds). Cambridge University Press.